International Journal of Material Forming (2024) 17:19
https://doi.org/10.1007/s12289-024-01813-3

ORIGINAL RESEARCH

Novel finite element model of analyzing wall thickness during tube drawing considering raw tube's thickness non-uniformity and die misalignment

N. A. Razali[1] · J. B. Byun[2] · M. S. Joun[2]

Received: 15 December 2022 / Accepted: 3 October 2023 / Published online: 6 March 2024

Abstract
Conventional engineering analyses for tube drawing processes have assumed an ideal material with uniform initial tube thickness; however, these assumptions limit the ability to address quality issues in the manufacturing industry. In this study, we present a finite element analysis model to analyze the tube drawing process with non-uniformity of the initial tube thickness and misalignment of the drawing die, using the implicit elastoplastic finite element method with a multibody treatment scheme (MBTS). We specifically focus on tube eccentricity. The plug in the MBTS is regarded as a deformable body with any fixed boundary condition in the lateral direction. Our analysis results show that an adequately tilted drawing die substantially reduces the eccentricity and thickness non-uniformity. The predictions are validated by comparison with experimental results in the literature.

Keywords Implicit elastoplastic FEM · Multibody treatment scheme · Non-uniform initial thickness · Tilted die · Tube drawing · Tube eccentricity

Introduction

Seamless tubes are fundamental materials for many industries, with numerous mechanical applications [1–3]. The fabrication process for seamless tubes begins with roll-piercing [4], extrusion [2, 5], and rolling [6] of the initial material, followed by cold drawing to create the tube. Preform materials may be geometrically and mechanically poor because of thickness non-uniformity, shape ovality, and non-homogeneous residual stress.

In industrial applications, some eccentricity is allowed; however, the consumption of the material becomes inefficient because the thickness specification is determined by the minimum thickness. The eccentricities of industrial tubes are between 1 and 3% for aluminum, up to 5% for copper, and up to 10% for steel [2, 5, 7] as defined by the difference between the maximum and minimum external diameters of the tube per its mean external diameter [2]. These geometrical and mechanical features are inevitable during fabrication because the tool (e.g., the plug) does not allow flexible control during pre-work step.

Additionally, non-homogeneous residual stresses can cause a decrease in structural strength and local metallurgical weakness during service and tube drawing. Residual stress may induce buckling of cylindrical tubes [8], and severe residual stresses may increase manufacturing costs during post-work surface or heat treatments intended to improve the formability and crack resistance of the final product. In contrast, improvements in non-homogeneity of the drawn tubes are useful to process engineers because consumer demand steadily pushes tube manufacturers to reduce tube weight and cost. This demand is expected to grow with existing efforts to combat global warming and improve material strength and use efficiency.

Tube drawings with various types of plugs have thus been studied in multiple ways [8–11]. Neves et al. [9] attempted to identify the best die and plug geometry to reduce the drawing force using a finite element method (FEM). Kuboki et al. [10] studied the effect of a plug on

✉ M. S. Joun
msjoun@gnu.ac.kr

[1] School of Mechanical and Aerospace Engineering, Gyeongsang National University, Gyeongsangnam-Do, Jinju-City 52828, South Korea

[2] Engineering Research Institute, School of Mechanical and Aerospace Engineering, Gyeongsang National University, Gyeongsangnam-Do, Jinju-City 52828, South Korea

residual tube stress by drawing tubes to determine the minimum bare reduction in thickness that is needed to level out and reduce residual stress. Yoshida et al. [11] experimentally and numerically studied fine tube drawing, with an emphasis on fixed and floating plugs. Linardon et al. [12] conducted experimental analyses of a tube drawing process with a long conical plug, then presented a numerical model with a pressure-dependent friction model. However, it is difficult to address geometrical and mechanical insufficiencies with conventional cold tube drawing because the plug is nearly always free to move.

Most research investigations have been based on the idealization of symmetry or perfection of the starting materials and dies or tools. Yoshida et al. [13] experimentally and numerically studied the tube drawing of Ni–Ti shape-memory alloy for medical applications, emphasizing the usage of a plug to improve the surface quality of the drawn tube. Palengat et al. [14] experimentally and numerically studied the drawing process of thin-walled 316L stainless steel tubes for medical applications. Alexandrova [15] analytically studied the failure of incompressible, rigid perfectly plastic material during drawing processes using Hill's general method and a fracture criterion based on a workability diagram. Rubio [16] conducted an analytical study of tube drawing using various theoretical approaches. Lee et al. [17] studied the causes of material fracture during cold tube drawing using a rigid-plastic FEM and the theory of ductile fracture.

Palengat et al. [18] presented an analysis model to accurately predict the drawing process, with an emphasis on hypothesis, physical modeling (flow behavior, tool behavior, and friction), and numerical modeling (load, meshing, friction, and convergence). Rubio et al. [19] analytically studied the tube drawing process, with an emphasis on the effects of input parameters (e.g., material flow behavior, die conical angle, area reduction, and friction conditions) on the process and product using an upper bound method. Boutenel et al. [20] presented a model for predicting the final dimensions of the tube with high accuracy in the cold tube drawing process. They provided some detailed information regarding the finite element (FE) model, including geometry, materials, boundary conditions, mesh, and numerical factors.

Pirling et al. [2] measured the residual strain of a cold-drawn copper tube using neutron diffraction to resolve the interconnection between the geometrical changes in the tubes caused by deformation non-homogeneity and the resulting residual stresses. Gattmah et al. [21] developed a technique for the measurement of residual stress for drawn tubes; the approach was validated by a comparison of FE predictions and X-ray diffraction results.

Béland et al. [22] conducted process design optimization of a drawing process in terms of the drawing force or maximum stress level to reduce the number of drawing stages (passes). Sheu et al. [23] optimized the profiles of the drawing die orifice and the plug, in terms of both drawing force and strain non-homogeneity, using the Taguchi method with the FEM. Hosseinzadeh and Mouziraji [24] attempted to identify optimal combinations of drawing parameters in terms of drawing force and thickness distribution in the round-to-square tube drawing. They also studied the optimization of process design parameters using an FEM with an optimization technique. Jafari et al. [25] presented an optimization approach that combined the Taguchi method and FEM for tube drawing; their approach identified the minimum forming force necessary to produce the minimum dimensional error. Farahani et al. [26] presented an optimized curved die profile for tube drawing that used a fixed conical plug to minimize the necessary tensile stress or drawing force and to reduce the stresses exerted on the die and plug; these effects were based on the appropriate determination of flow behavior of the material, area reduction, plug angle, and friction conditions.

However, few researchers have studied tube drawing via realistic tube drawing processes with non-uniform thicknesses and/or non-idealized tools or dies. Tetley [27] reported that the drawn tube could be significantly improved during block tube drawing, depending on the initial eccentricity of the tube and reduction in the area of the drawing process. Pirling et al. [3] studied the effects of wall thickness, eccentricity, ovality, and residual stress in tube drawing on tube qualities using a three-dimensional FEM. Foadian et al. [7] experimentally and numerically studied the effects of tilting the die and shifting the tube on the resulting tube eccentricity and residual stresses, using as-received tubes with eccentricity; they showed that a tilted die improves product quality with respect to residual stresses. Al-Hamdany et al. [5] conducted experimental analyses of the effect of a tilted die in tube drawing on the texture, dislocation density, and mechanical properties of the drawn tube; they concluded that the method of tilting the drawing die is effective for controlling tube eccentricity.

This study presented a finite element analysis model to investigate the tube drawing process characterized by a tilted drawing die and non-uniform raw tube thickness using an implicit elastoplastic FEM and a multibody treatment scheme (MBTS [28]). MBTS treated the contact condition between the tube and plug using the penalty method. The plug was regarded as a laterally movable and deformable body to consider its movement and vibration inside the tube. However, its rotational motion was

constrained. The thickness distribution of the prediction was compared with experimental results found in the literature, and the effects of bearing length were analyzed. Our analysis results showed that bearing length and tilted angle strongly affect the eccentricity of the tube produced by tube drawing.

FE modelling

Definition of process

Al-Hamdany et al. [5] experimentally studied the drawing process of a copper tube with a ± 5° tilted die; a schematic diagram of the + 5° tilted die case is shown in Fig. 1. The extruded and annealed copper tube (outer diameter: 65.0 mm; mean thickness: 5.5 mm) was investigated. In this study, we used the tube drawing process described by Al-Hamdany et al.; our results were numerically studied and compared with their experimental results. The non-uniform thickness of the initial tube only at the cross-section was considered. Following Al-Hamdany et al.'s work, the minimum and maximum thicknesses of the initial tube were purposely fixed at 5.14 and 5.78 mm, respectively, which were defined by the eccentricity, i.e., the gap between the central lines of inner and outer circles of the tube cross-section. Importantly, the maximum thickness is located on the opposite side of the *x*-direction for all figures presented in this paper.

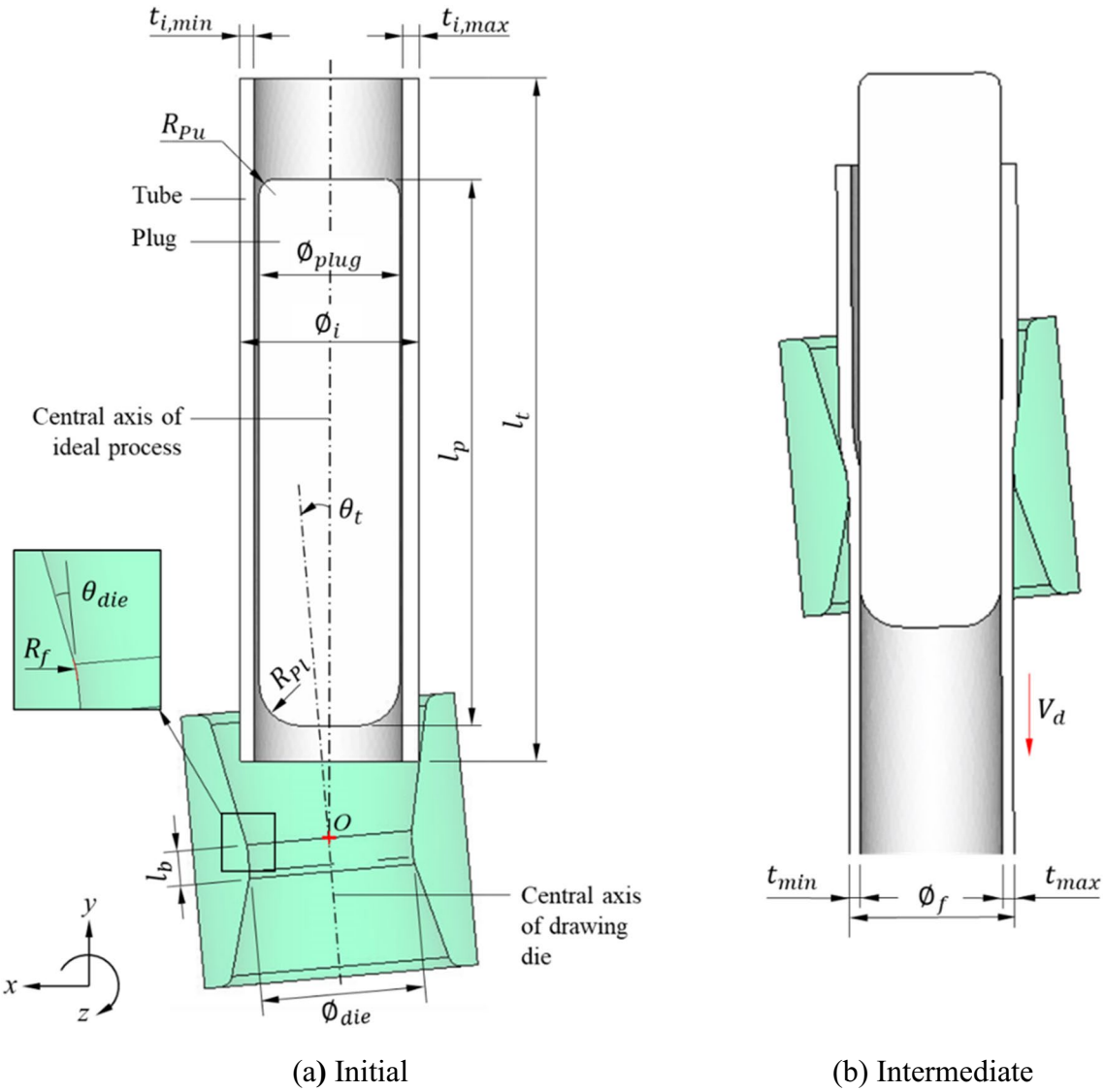

Fig. 1 Schematic diagram of tube drawing process studied

The tube was assumed to behave as an elastoplastic material. A three-dimensional FE model (i.e., a half model) was developed for the tube drawing process by adaptation of an implicit elastoplastic FEM with the MBTS. In the work of Al-Hamdany et al., three main parameters were not described or considered: bearing length of the die, denoted as l_b; fillet radius of the die's inner corner, denoted as R_f; and friction coefficients. Point O on the drawing die in Fig. 1 is the center of rotation when the die is tilted clockwise or counterclockwise. In this study, the drawing velocity V_d was fixed at 1.0 mm/s because the material was assumed to be rate-independent. Additionally, the friction coefficient between the tube and plug, and between the tube and die, was assumed to be 0.05 [29–31]. Dies with different bearing lengths and fillet radii, l_b and R_f, varying from 5–20 mm and 0.5–30 mm, respectively, were used to investigate the effects of these parameters on the thickness distribution after tube drawing. Table 1 summarizes the key dimensions of the process studied.

Table 2 shows the material and flow properties of the tube and plug. The flow function of the copper tube was characterized using a generalized blending flow model [32] from the reference flow curve (RFC) described by the selected points from O to T, as shown in Fig. 2. The RFC was obtained using the method of Joun et al. [30] from the experimental tensile test curve, as shown in the lower panel of Fig. 2, given by Al-Hamdany et al. [5]. The dashed line in the lower panel of Fig. 2 is the theoretical tensile test curve predicted using the generalized blending flow model, which implies that it is accurate. Note that point N ($\varepsilon_t = 0.41$) on the flow curve (true stress–strain curve) is corresponds to the necking point N_e ($\varepsilon_e = 0.50$) on the engineering stress–strain curve. The experimental flow curve from N to T describes the post-necking strain hardening. It is also noted that the predicted engineering stress–strain curve is in good agreement with the experiments, as can be shown in the lower panel of Fig. 2. However, it can be seen that the flow curve is remarkably different from the engineering stress–strain curve, compared with the forgeable steels including SCM415, SCM435, and SWCH10A [33]. The reason for such a big difference lies in the significant elongation of the material, like stainless steel [34]. The initial effective strain of the tube was assumed to be 0.1 to satisfy the value of 124 MPa for its initial flow stress.

Table 1 Key dimensions of initial tube drawing process [5]

Parameters	Units	Values
Minimum initial tube thickness,$t_{i,min}$	mm	5.14
Maximum initial tube thickness,$t_{i,max}$	mm	5.78
Initial tube diameter,$\varnothing_i$	mm	65.0
Plug diameter,$\varnothing_{plug}$	mm	51.0
Die orifice diameter,$\varnothing_{die}$	mm	60.0
Half conical die angle,θ_{die}	Deg. (°)	12.0
Tilted angle,θ_t	Deg. (°)	±5.0
Length of tube,l_t	mm	250
Length of plug,l_p	mm	200
Upper corner radius of plug,R_{Pu}	mm	5
Lower corner radius of plug,R_{Pl}	mm	15

Table 2 Material properties of tube material and plug [5]

Parameters	Units	Values
Plug (SKD 11)		
Young's modulus,E	GPa	200.0
Poisson's ratio,ν	–	0.24
Flow function	MPa	$\tilde{\sigma} = 2630(1+\bar{\varepsilon}/0.01)^{0.16}$
Tube (Copper)		
Young's modulus,E	GPa	130
Poisson's ratio,ν	–	0.34
Flow function	MPa	$\tilde{\sigma} = \sum_{i=1}^{4} \alpha_i S_i$
		$S_1 = 124(1+\bar{\varepsilon}/0.045)^{0.450}, \alpha_1 = -1.62$ $S_2 = 174(1+\bar{\varepsilon}/0.170)^{0.575}, \alpha_2 = 18.11$ $S_3 = 191(1+\bar{\varepsilon}/0.295)^{0.700}, \alpha_3 - 25.81$ $S_4 = 200(1+\bar{\varepsilon}/0.420)^{0.825}, \alpha_4 = 10.33$

Because of the difficulty of placing the plug in the correct position, the material and plug were assumed to simultaneously move towards the orifice until the process reaches the steady-state condition. The bottom side of the material and plug were regarded as velocity-prescribed boundaries in the drawing direction until the plug reached its target position.

The floating plug has a significant effect on correction for misalignment errors that affect tube quality. Figure 3 shows the FE model; here, the importance of the modeling technique of the plug is emphasized under the conditions of non-axisymmetric tube drawing, along with die misalignment

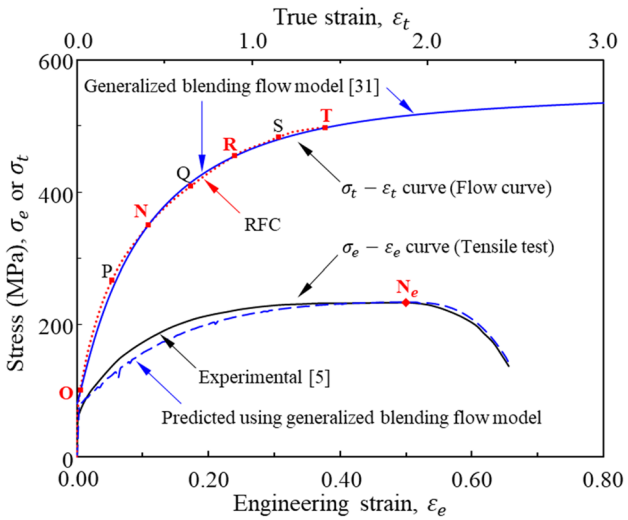

Fig. 2 Flow information of the copper

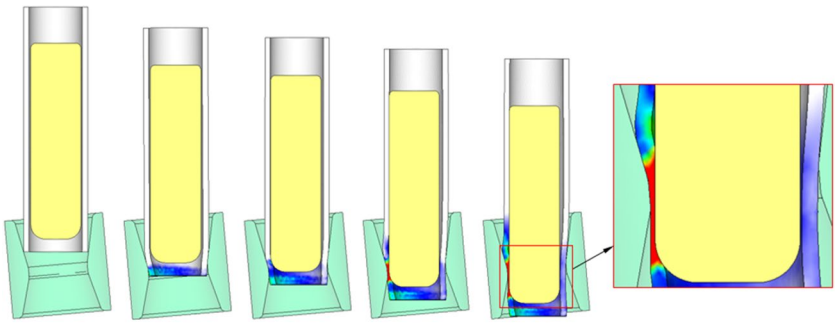

(a) Fixed and rigid plug

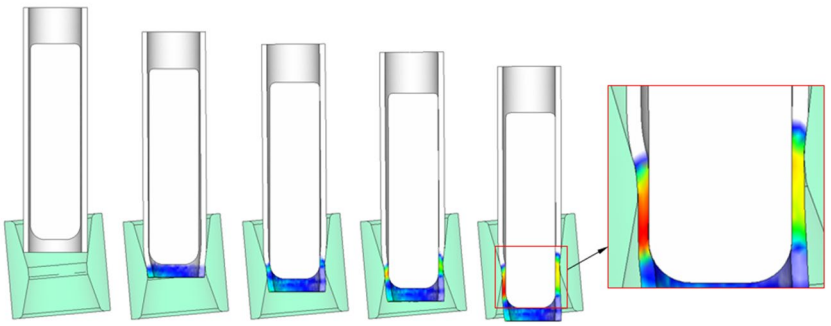

(b) Laterally movable and deformable plug

Fig. 3 History of deformation with effective strain (+5° tilted die case)

and tube thickness non-uniformity. The drawing die was assumed to be rigid, whereas the plug was regarded as a laterally movable and deformable (elastic–plastic) body. However, the plug was regarded as a laterally fixed and rigid body only as an exceptional case in Fig. 3a. The predicted histories of the deformation and the effective strain of the tube drawing process for both rigid and deformable plugs are shown in Fig. 3a and b, respectively.

In Fig. 4, the laterally movable and deformable plug moves towards the right side because of the need for force equilibrium. This demonstrates that the treatment scheme of the plug is a critical consideration during non-axisymmetric tube drawing. Notably, there is no actual axisymmetric drawing because of the eccentricity of the initial tube.

FE predictions of tube drawing processes with a tilted die

Numerical effects on predictions

We assumed a plane of symmetry for the tube drawing process. First, the numerical effects were assessed using various FE mesh systems [35]. The same die and process conditions were used. For this purpose, the effects of the number of tetrahedral elements on tube reference diameter and eccentricity were investigated. The reference diameter, denoted as $\varnothing_f$ as shown in Fig. 1b, is the predicted distance of the two external surfaces of the drawn tube on the symmetric plane. The eccentricity, denoted as e, is defined as follows:

$$e = \frac{t_{max} - t_{min}}{t_{max} + t_{min}}, \tag{1}$$

where t_{max} and t_{min} are the maximum and minimum thicknesses of the drawn tube, respectively.

The tube drawing process of Al-Hamdany et al. [5] was conducted using the initial tube diameter of 65.0 mm, and minimum and maximum thicknesses of 5.14 and 5.78 mm, respectively, as summarized in Table 1. The initial tube eccentricity was 5.86%. All predicted tube thicknesses and diameters used in this study were obtained after springback analyses. Figure 5 shows the FE mesh systems constructed with the lowest (39,000) and highest (142,000) tetrahedral elements tested for both the plug and tube material.

In Fig. 6, the e-values slightly decreased as the number of tetrahedral FEs increased, up to approximately 90,000; subsequently, the e-values generally remained constant. When 39,000 tetrahedral elements were used, the maximum predicted eccentricity was 4.41%; when 89,000

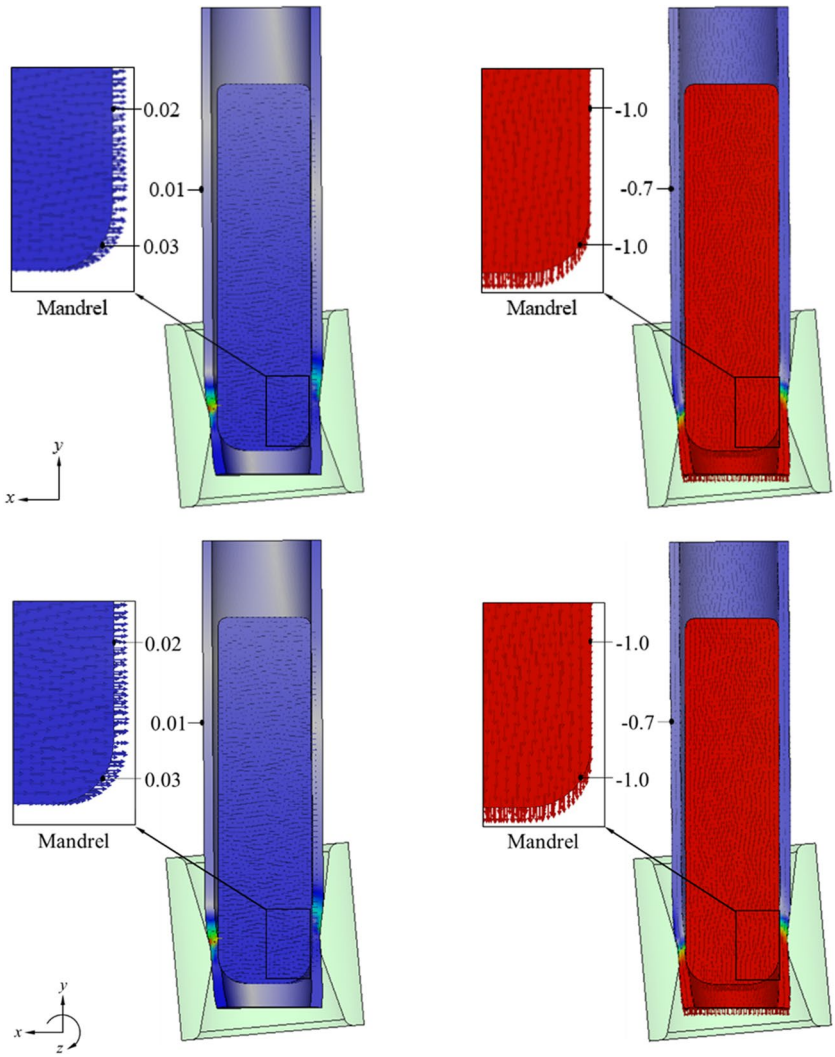

(a) x-direction (b) y-direction

Fig. 4 Nodal velocity components of tube material and plug [mm/s] (+5° tilted die case)

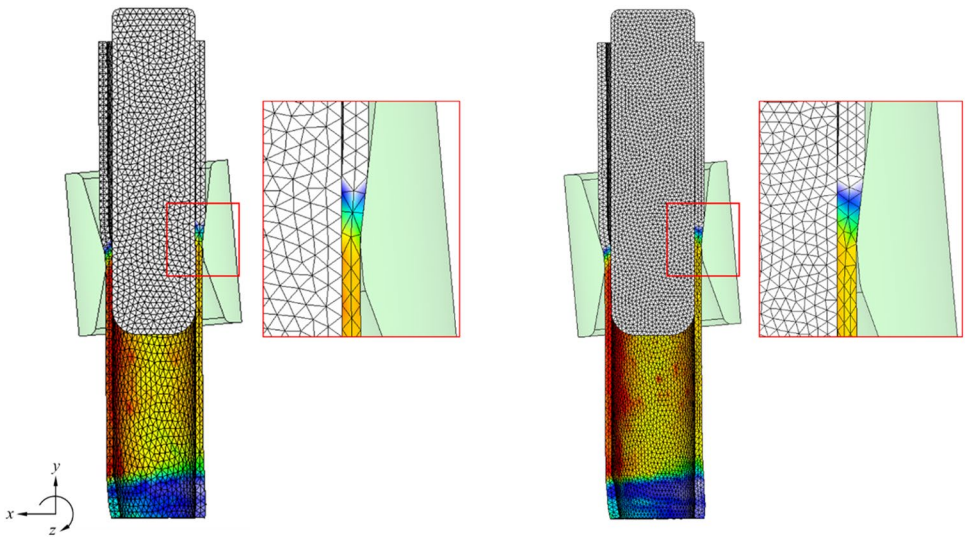

(a) 39,000 tetrahedral elements (b) 142,000 tetrahedral elements

Fig. 5 FE mesh systems of half FE model (+5° tilted die case)

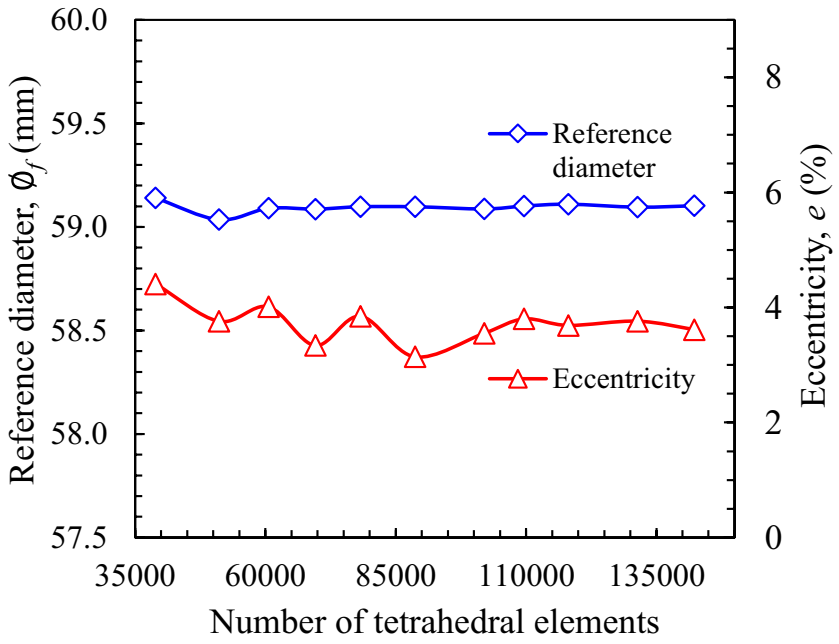

Fig. 6 Effects of the number of tetrahedral elements on the eccentricity and reference diameter of the drawn tube

tetrahedral elements were used, the minimum predicted eccentricity was 3.14%. Figure 6 shows that as the number of tetrahedral FEs approached 90,000, the predicted e-values became more stable and reliable, as revealed in a previous study [36] regarding the FE simulation of a rotary tube-draw bending process. In contrast, the reference diameter $\varnothing_f$ became stable beginning at 60,000 tetrahedral elements. An FE mesh system with approximately 100,000 tetrahedral elements was thus used for all FE models in this study.

Effects of bearing length and fillet radius on eccentricity

The bearing length, l_b, and the fillet radius of the die's inner corner,R_f, have significant influences on the drawing phenomena for non-axisymmetric tube drawing, particularly when a tilted drawing die is involved. These effects occur because the tilted angle directly affects the reduction of the area.

In accordance with the work of Al-Hamdany et al. [5], t_{max} and t_{min} after the first pass, in the case of die tilted + 5°, were 4.63 and 4.35 mm, respectively. Therefore, the e-value experimentally determined from the literature was 3.42%; this value was used in our numerical study. However, because Al-Hamdany et al. did not provide any details regarding l_b and R_f, we selected four l_b values (5, 10, 15, and 20 mm) and three R_f values (0.5, 10, and 30 mm) for our simulation of the non-axisymmetric tube drawing process. Figures 7 and 8 show two examples of assumed dies using the selected l_b and R_f values, respectively, with an emphasis on the projected die orifice distance on the symmetric plane, denoted as $\varnothing_p$; importantly, $\varnothing_p$ is similar to $\varnothing_f$ in the figures.

Figure 9 shows the variation in the reference diameter of the drawn tubes with l_b and R_f, indicating that the mean outer diameter of a tube drawn by the tilted die may decrease when the bearing length increases or the fillet radius decreases.

Figure 10 shows the bearing length–eccentricity curve of the process with the + 5° tilted die for fillet radii of 0.5, 10, and 30 mm. Notably, it was calculated after the prediction of springback because the tube drawing process is considerably affected by the springback phenomenon [23, 24]. Eccentricity linearly decreased with bearing length, except for the shortest bearing length, and a distinct minimum point at the bearing length of approximately 10 mm was observed for all fillets.

Eccentricity is primarily affected by bearing length when a tilted die is used because it determines the $\varnothing_p$ value or the area reduction. This relationship is depicted in Figs. 7 and 8, implying that a tilted die with an appropriate bearing length should be used to reduce the eccentricity of drawn tubes. Figure 11 shows the changes in traction and material–die interface according to bearing length in the + 5° tilted die case, indicating that contact discontinuity varies according to bearing length. Notably, contact on the thicker side is not affected by the bearing length, whereas contact on the thinner side is affected. These findings suggest that contact discontinuity is a primary factor influencing thickness uniformity.

Considering that the tube was initially in contact with the die at the left side (i.e., thicker wall), the tube tended to move towards the x-direction. Inwardly, the plug used for

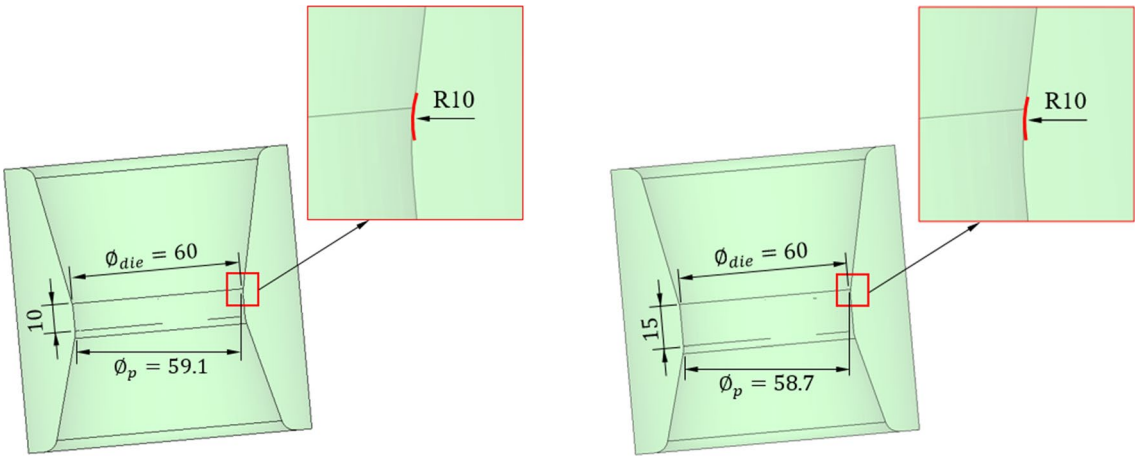

(a) $l_b = 10, R_f = 10$ (b) $l_b = 15\ , R_f = 10$

Fig. 7 Schematic diagrams of drawing dies using different l_b values, with an emphasis on $\emptyset_p$ [mm]

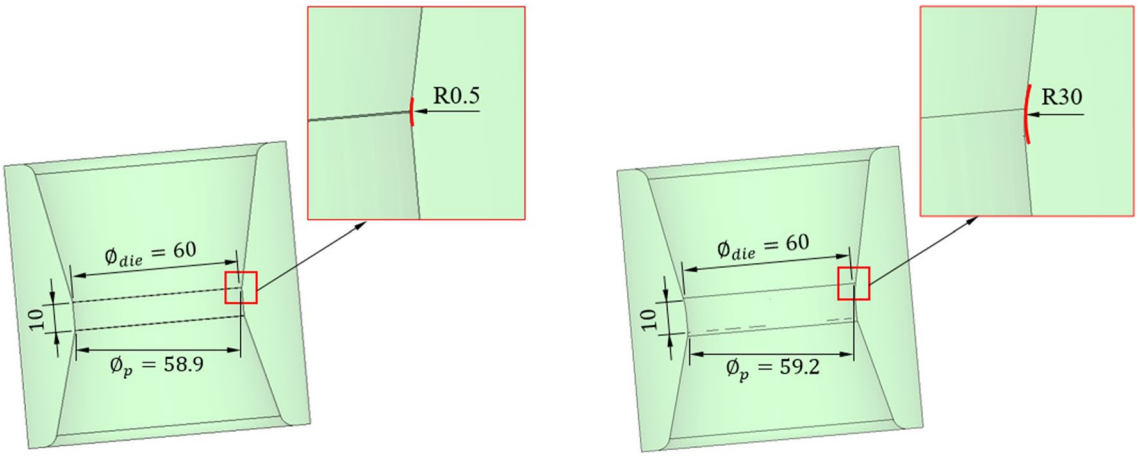

(a) $l_b = 10, R_f = 0.5$ (b) $l_b = 10, R_f = 30$

Fig. 8 Schematic diagrams of drawing dies using different R_f values, with an emphasis on $\emptyset_p$ [mm]

this process was being pushed in the same direction. This relationship explains the higher value of traction force and effective strain on the right side in all tubes in Figs. 11 and 12, respectively.

In Fig. 12, the material in the entry side was bent to the left in the case of a 5-mm bearing length and to the right in cases of 15- and 20-mm bearing lengths when it was observed towards the negative z-axis; material alignment was maintained in the case of a 10-mm bearing length.

Furthermore, all bearing lengths produced similar effective strain distribution patterns: larger effective strain of the drawn tube on the thinner side than on the thicker side, and minimum effective strain at the middle between the two sides (except in the case with the lowest bearing length). The larger effective strain on

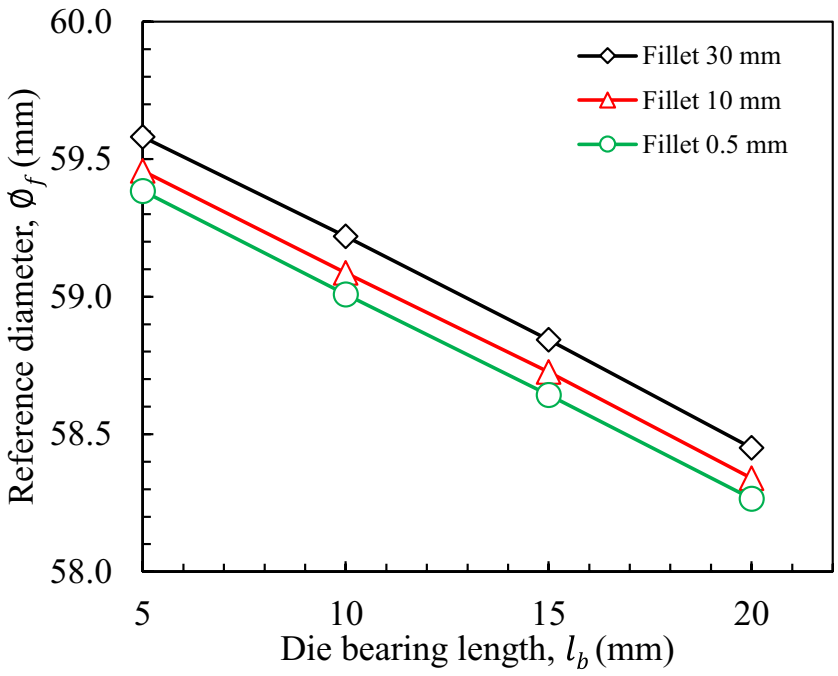

Fig. 9 Predicted reference diameters, $\varnothing_f$ with different l_b and R_f for the + 5° tilted die cases

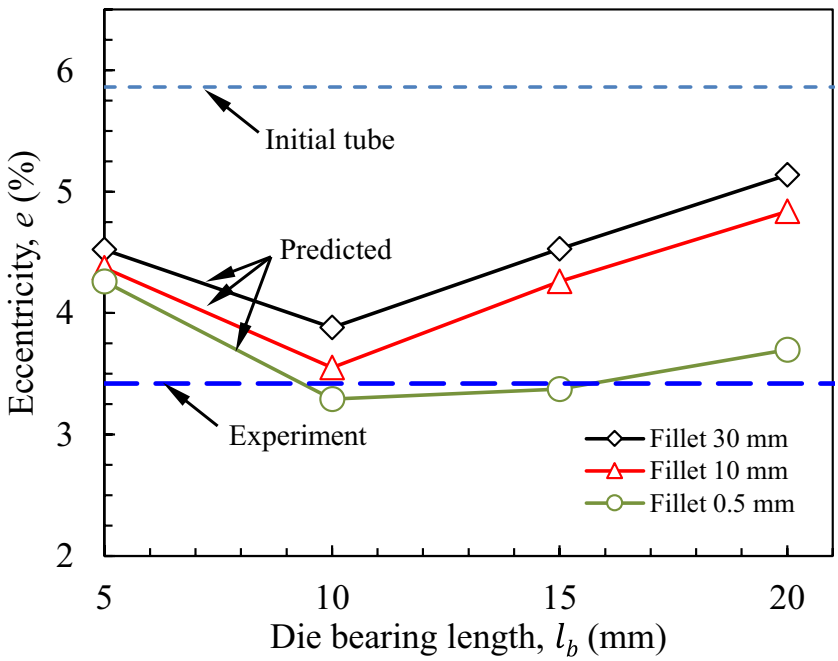

Fig. 10 Bearing length–eccentricity curve with different l_b and R_f values for the + 5° tilted die case

the thinner side presumably led to improved thickness uniformity (i.e., reduction in eccentricity). As indicated by the effective strain rate distribution in Fig. 13, the material point passed through a longer distance on the thinner side than on the thicker side because the material in the exit side leaned to the right. The 15- and 20-mm bearing length cases exhibited a large difference in effective strain rate between the middle point and the thicker side, potentially leading to deterioration of the thickness uniformity of the drawn tube, compared with the 10-mm bearing length case.

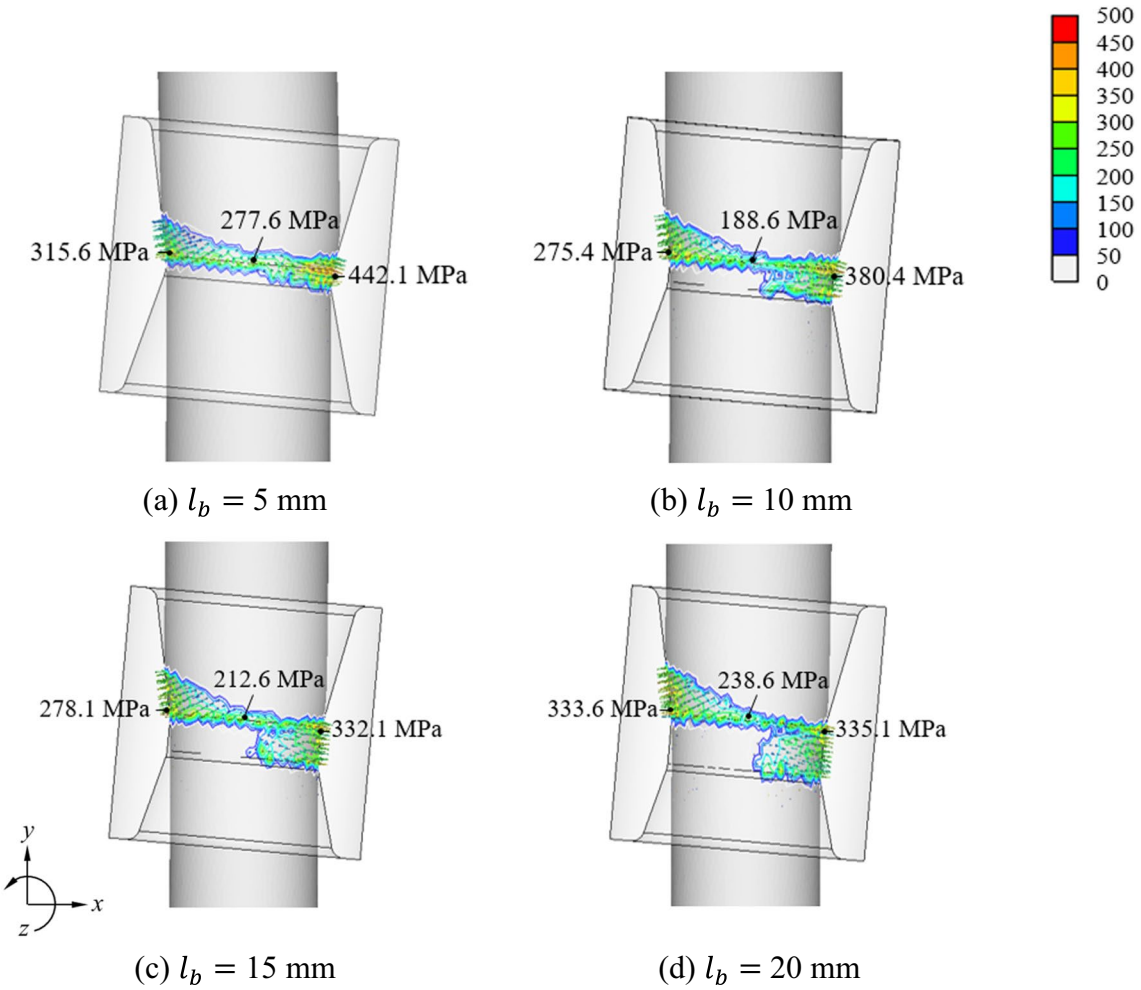

(a) $l_b = 5$ mm (b) $l_b = 10$ mm

(c) $l_b = 15$ mm (d) $l_b = 20$ mm

Fig. 11 Tube traction for different l_b($R_f = 10$ mm, + 5° tilted die)

Notably, the projected lengths of the material–die contacts on the symmetric plane varied according to bearing length, indicating that the 10-mm bearing length case exhibited minimum and maximum projected lengths on the left and right sides, respectively, when they were observed in the negative z-axis direction. These findings are related to the minimum eccentricity at the bearing length of 10 mm, as shown in Fig. 10.

Experimental validation of predictions

In accordance with the work of Al-Hamdany et al. [5], the drawing die was tilted in two directions: clockwise and counterclockwise, denoted as − 5° and + 5°, respectively. The experiments by Al-Hamdany et al. indicated that the direction of the tilted die significantly affects the thickness distribution. When the die angle was reduced on the thinner side, as shown in Fig. 14a, the eccentricity worsened. In contrast, when the die angle was reduced on the thicker side, as shown in Fig. 14b, the eccentricity improved. As the angle on one side decreased, the angle on the other side increased.

Bearing length and fillet radius have a direct influence on the outer diameter of the drawn tube because the $\varnothing_p$ value affects the reduction of the area. However, there was no detailed information regarding die geometries, such as die bearing length and fillet radius, in the work by Al-Hamdany et al. Identical values were provided for both the initial orifice diameter and outer diameter of the drawn tube in the misaligned tube drawing process with the ± 5° tilted die. Because the present study was intended to determine the mechanism underlying reduction of the eccentricity of the

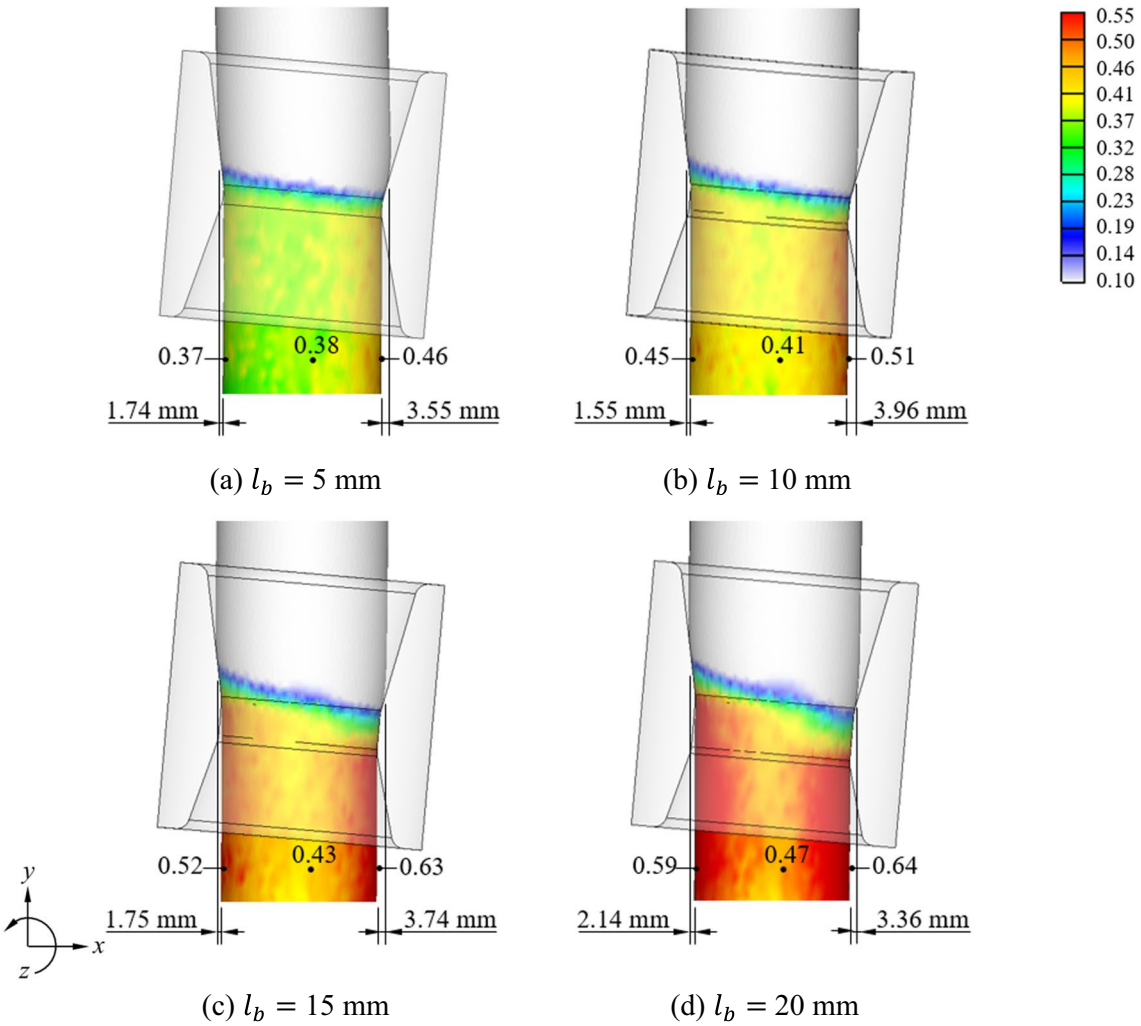

Fig. 12 Effective strain of drawn tube for different l_b($R_f = 10$ mm, + 5° tilted die)

drawn tube, the initial orifice diameter and fillet radius were assumed to be 60.8 and 10 mm, respectively, which produced an outer diameter nearly identical to the experiments.

Table 3 summarizes and compares the predicted and experimental results for the cases mentioned above. The bearing lengths and inner corner radii used for both cases were 10 mm. Table 3 shows that the *e*-value of the tube drawn by the − 5° tilted die increased by approximately 2.3% from the initial tube (i.e., the eccentricity worsened). In contrast, the *e*-value of the tube drawn by the + 5° tilted die decreased by approximately 2.4%. Surprisingly, the maximum percentage error between the predictions and experiments of the wall thickness and eccentricity was 3.31%, indicating that the predictions were accurate.

Conclusions

We conducted a numerical study of the tube drawing process, in which die misalignment was assumed because of a tilted die and thickness non-uniformity in the initial tube. An implicit elastoplastic FEM was used, along with an MBTS. We simulated an example tube drawing process in the literature, characterized by its initial tube with 5.86% eccentricity and ± 5° tilted die angle, and compared the predicted results with experimental findings.

Because a tilted die causes an extensive change in the lateral force exerted on the plug, a novel FE model was presented based on the MBTS in which the plug was modeled as an elastically deformable and rigidly movable

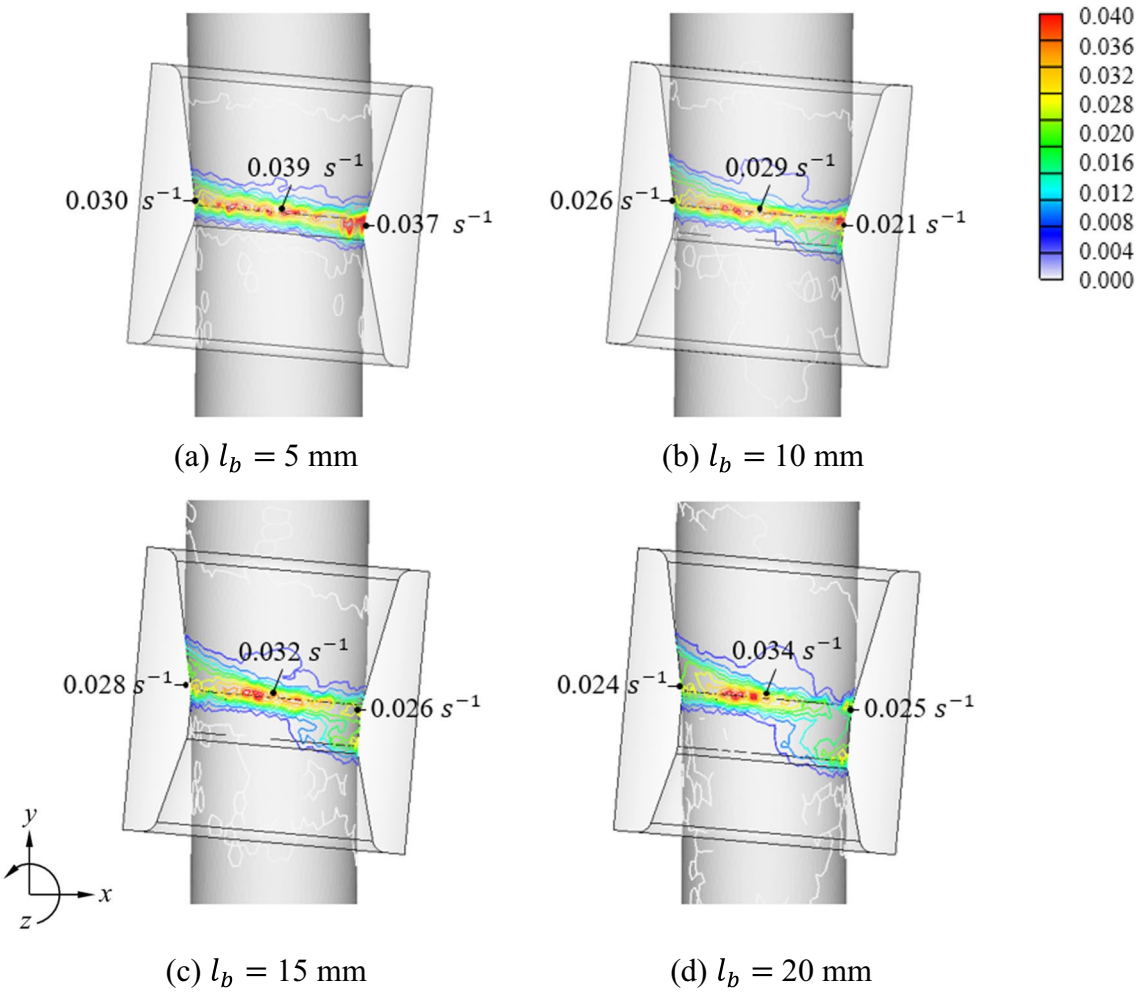

Fig. 13 Effective strain rate of drawn tube for different l_b($R_f = 10$ mm, +5° tilted die)

material. The numerical effects of FE mesh systems on the predictions were assessed, revealing that the half FE model with approximately 100,000 tetrahedral elements for both the plug and tube material is robust in terms of numerical effects.

The bearing length l_b and the fillet radius R_f played essential roles in controlling the thickness distribution, as well as the reference diameter of the tube $\varnothing_f$ in non-axisymmetric tube drawing using the tilted die and non-uniform initial tube. Numerical analysis revealed that the predicted $\varnothing_f$ linearly decreases as the bearing length increases when the bearing length exceeds a low threshold value. Moreover, an optimal bearing length minimizes the eccentricity, depending on the initial eccentricity of the tube material and the degree of die misalignment. In this study, the optimal l_b and R_f for the process studied were both 10 mm when the + 5° tilted die was used. The maximum errors between predictions and experiments for wall thicknesses and eccentricity were very small.

Researchers often overlook tube non-uniformity and eccentricity when conducting numerical analyses of tube drawing processes. However, these issues are becoming increasingly crucial in minimizing material consumption and protecting the environment. This study provides a deeper understanding of the non-axisymmetric tube drawing process with die misalignment and initial tube thickness non-uniformity. It isn't easy to improve thickness uniformity during tube drawing because of the characteristics of the tube drawing process. This study provides insights into the development of novel drawing processes and technologies for the fabrication of high-quality tubes, while contributing to green manufacturing practices in an effort towards net-zero emissions.

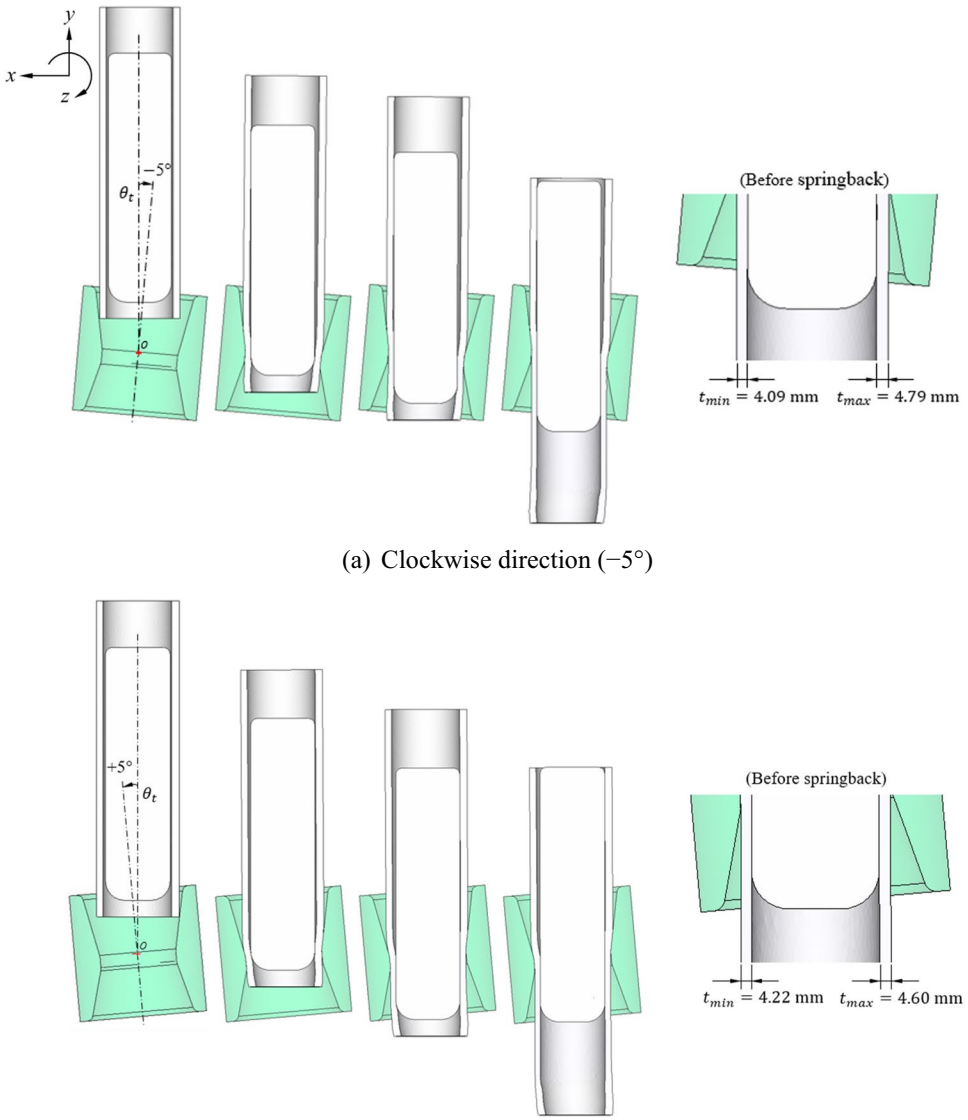

Fig. 14 Predicted history of plastic deformation during tube drawing using the ± 5° tilted angle

Table 3 Experiment and prediction results

Tube	Diameter, ∅ (mm)	Wall thickness (mm)		Eccentricity, e (%)
		t_{max}	t_{min}	
Initial	65	5.78	5.14	5.86
Die tilted − 5°				
Experiment [5]	60	4.84	4.14	7.85
Prediction	59.93	4.81	4.09	8.11
Error (%)	0.12	0.62	1.21	3.31
Die tilted + 5°				
Experiment [5]	60	4.63	4.35	3.42
Prediction	59.93	4.60	4.29	3.44
Error (%)	0.12	0.65	1.38	0.58

Acknowledgements This work was supported Korea Institute of Energy Technology Evaluation and Planning (KETEP) grant funded by the Korea government (MOTIE) (20214000000520, Human Resource Development Project in Circular Remanufacturing Industry) and by "Regional Innovation Strategy (RIS) (2021RIS-003)" through the National Research Foundation of Korea(NRF) funded by the Ministry of Education(MOE).

Data availability The datasets generated and/or analyzed during the current study are available from the corresponding author on reasonable request.

Code availability The data that support the findings of this study are available from the corresponding author and the information about the code can be found from the cited references.

Declarations

Ethical approval The submitted work is original, complete and has not been submitted or published elsewhere in any form or language. Human participants or animals were not involved in this part of work that requires any ethical approval.

Consent to participate Not applicable.

Consent to publish The author confirms that the work has not been published before; that it is not under consideration for publication elsewhere; that its publication has been approved by all co-authors; that its publication has been approved by the responsible authorities at the institution where the work is carried out. The authors provide their consent to publish the manuscript in the International Journal of Material Forming.

Competing interest The authors declare no competing interest.

References

1. Jansson M, Nilsson L, Simonsson K (2007) On process parameter estimation for the tube hydroforming process. J Mater Process Technol 190(1–3):1–1. https://doi.org/10.1016/j.jmatprotec.2007.02.050
2. Pirling T, Carradò A, Brück S, Palkowski H (2008) Neutron stress imaging of drawn copper tube: comparison with finite-element model. Metall and Mater Trans A 39(13):3149–3154. https://doi.org/10.1007/s11661-008-9629-8
3. Pirling T, Carradò A, Palkowski H (2011) Residual stress distribution in seamless tubes determined experimentally and by FEM. Procedia Eng 10:3080–3085. https://doi.org/10.1016/j.proeng.2011.04.510
4. Guo W, Chen R, Jin JJ (2015) Online eccentricity monitoring of seamless tubes in cross-roll piercing mill. J Manuf Sci Eng 137(2). https://doi.org/10.1115/1.4028440
5. Al-Hamdany N, Salih MZ, Palkowski H, Carradò A et al (2021) Tube Drawing with Tilted Die: Texture. Dislocation Density Mech Properties Metals 11(4):638. https://doi.org/10.3390/met11040638
6. Lambiase F, Di Ilio A (2012) Deformation inhomogeneity in roll drawing process. J Manuf process 14(3):208–215. https://doi.org/10.1016/j.jmapro.2011.12.005
7. Foadian F, Carradó A, Palkowski H (2015) Precision tube production: Influencing the eccentricity and residual stresses by tilting and shifting. J Mater Process Technol 222:155–162. https://doi.org/10.1016/j.jmatprotec.2015.03.008
8. Le Grognec P, Casari P, Choqueuse D (2009) Influence of residual stresses and geometric imperfections on the elastoplastic collapse of cylindrical tubes under external pressure. Mar Struct 22(4):836–854. https://doi.org/10.1016/j.marstruc.2009.09.003
9. Neves FO, Button ST, Caminaga C (2005) Gentile FC (2005) Numerical and experimental analysis of tube drawing with fixed plug. J Braz Soc Mech Sci Eng 27:426–431. https://doi.org/10.1590/S1678-58782005000400011
10. Akiyama M, Kuboki T (2002) Optimisation of method for reducing residual stresses after cold bar drawing. Ironmak Steelmak 29(2):101–106. https://doi.org/10.1179/030192302225001974
11. Yoshida K, Furuya H (2004) Mandrel drawing and plug drawing of shape-memory-alloy fine tubes used in catheters and stents. J Mater Process Technol 153:145–150. https://doi.org/10.1016/j.jmatprotec.2004.04.182
12. Linardon C, Favier D, Chagnon G, Gruez B (2014) A conical mandrel tube drawing test designed to assess failure criteria. J Mater Process Technol 214(2):347–357. https://doi.org/10.1016/j.jmatprotec.2013.09.021
13. Yoshida K, Watanabe M, Ishikawa H (2001) Drawing of Ni–Ti shape-memory-alloy fine tubes used in medical tests. J Mater Process Technol 118(1–3):251–255. https://doi.org/10.1016/S0924-0136(01)00930-X
14. Palengat M, Chagnon G, Favier D, Louche H, Linardon C, Plaideau C (2013) Cold drawing of 316l stainless steel thin-walled tubes: experiments and finite element analysis. Int J Mech Sci 70:69–78. https://doi.org/10.1016/j.ijmecsci.2013.02.003
15. Alexandrova N (2001) Analytical treatment of tube drawing with a mandrel. Proc Inst Mech Eng, Part C: J Mech Eng Sci 215(5):581–589. https://doi.org/10.1243/09544060115209
16. Rubio EM (2006) Analytical methods application to the study of tube drawing processes with fixed conical inner plug: Slab and upper bound methods. J Achiev Mater Manuf Eng 14(1–2):119–130
17. Lee SK, Ko DC, Kim BM, Lee JH, Kim SW, Lee YS (2007) A study on monobloc tube drawing for steering input shaft. J Mater Process Technol 191(1–3):55–58. https://doi.org/10.1016/j.jmatprotec.2007.03.062
18. Palengat M, Chagnon G, Millet C, Favier D (2007) Tube drawing process modelling by a finite element analysis. AIP Conf Proc 908(1):705–710. https://doi.org/10.1063/1.2740893
19. Rubio EM, Camacho AM, Pérez R, Marín MM (2017) Guidelines for selecting plugs used in thin-walled tube drawing processes of metallic alloys. Metals 7(12):572. https://doi.org/10.3390/met7120572
20. Boutenel F, Delhomme M, Velay V, Boman R (2018) Finite element modelling of cold drawing for high-precision tubes. C R Méc 346(8):665–677. https://doi.org/10.1016/j.crme.2018.06.005
21. Gattmah J, Ozturk F, Orhan S (2020) A new development of measurement technique for residual stresses generated by the cold tube drawing process with a fixed mandrel. The Int J Adv Manuf Technol 108(11):3675–3687. https://doi.org/10.1007/s00170-020-05645-8
22. Béland JF, Fafard M, Rahem A, D'Amours G, Cote T (2011) Optimization on the cold drawing process of 6063 aluminium tubes. Appl Math Model 35(11):5302–5313. https://doi.org/10.1016/j.apm.2011.04.025
23. Sheu JJ, Lin SY, Yu CH (2014) Optimum die design for single pass steel tube drawing with large strain deformation. Procedia Eng 81:688–693. https://doi.org/10.1016/j.proeng.2014.10.061
24. Hosseinzadeh M, Mouziraji MG (2016) An analysis of tube drawing process used to produce squared sections from round tubes through FE simulation and response surface methodology. J Adv Manuf Technol 87(5):2179–2194. https://doi.org/10.1007/s00170-016-8532-5
25. Jafari M, Hosseinzadeh M, Elyasi M (2018) Optimization of tube drawing process through FE analysis, intelligent computation, and experimental verification. Proc Inst Mech Eng E: Process Mech Eng 232(1):94–107. https://doi.org/10.1177/0954408916685587
26. Farahani ND, Parvizi A, Barooni A, Naeini SA (2018) Optimum curved die profile for tube drawing process with fixed conical plug. The Int J Adv Manufactur Technol 97(1):1–1. https://doi.org/10.1007/s00170-018-1803-6
27. Tetley G (1978) Variation of eccentricity during block drawing of tubes. J App Metalwork 1(1):80–83. https://doi.org/10.1007/BF02833963
28. Joun MS, Chung SH, Lee MC, Eom JG, Chung WJ (2023) Cases of multi-body mechanics in metal forming. AIP Conf Proc 257(1):020003. https://doi.org/10.1063/5.0119123
29. Joun MS, Choi I, Eom J, Lee M (2007) Finite element analysis of tensile testing with emphasis on necking. Comput Mater

Sci 41(1):63–69. https://doi.org/10.1016/j.commatsci.2007.03.002
30. Joun MS, Eom JG, Lee MC (2008) A new method for acquiring true stress–strain curves over a large range of strains using a tensile test and finite element method. Mech Mater 40(7):586–593. https://doi.org/10.1016/j.mechmat.2007.11.006
31. Joun MS, Moon HG, Choi IS, Lee MC, Jun DB (2009) Effects of friction laws on metal forming processes. Tribol Int 42(2):311–319. https://doi.org/10.1016/j.triboint.2008.06.012
32. Jee CW, Ji SM, Byun JB, Joun MS (2022) Practical blended flow models for bulk metal forming using the cylindrical tensile test with its related flow behavior at large strain. J Korean Soc Precis Eng 39(8):583–593. https://doi.org/10.7736/JKSPE.022.037
33. Kang MK, Ji SM, Lee SW, Hong SM, Joun MS (2023) Flow behavior dependence of rod shearing phenomena of various materials in automatic multi-stage cold forging. J Mech Sci Technol 37:139–148. https://doi.org/10.1007/s12206-022-1214-3
34. Byun JB, Razali MK, Lee CJ, Seo ID, Chung WJ, Joun MS (2020) Automatic multi-stage cold forging of an SUS304 ball-stud with a hexagonal hole at one end. Materials 13(22):5300. https://doi.org/10.3390/ma13225300
35. Lee MC, Joun MS, Lee JK (2007) Adaptive tetrahedral element generation and refinement to improve the quality of bulk metal forming simulation. Finite Eleme Anal Des 43(10):788–802. https://doi.org/10.1016/j.finel.2007.05.006
36. Razali NA, Chung SH, Chung WJ, Joun MS (2022) Implicit elastoplastic finite element analysis of tube-bending with an emphasis on springback prediction. J Adv Manuf Technol 120(9):6377–6391. https://doi.org/10.1007/s00170-022-09073-8